r_i = total rate of formation of product i; that is, rate summed for all wave lengths, g.moles/(cc.)(sec.)
r_d = total rate of decomposition of acetone, g.moles/(cc.)(sec.)
$\bar{r}_d$ = average, total rate over reactor cross section
$\bar{r}_{d,c}$ = $f\,\bar{r}_d$
T_λ = fraction of light of wave length, λ, transmitted through all filter solutions
V = irradiated volume of reactor, cc.
α_λ = absorptivity of acetone; in tables units are 1/(g.moles)(cm.); in equations sq. cm./(g.mole) is used. All values based upon intensity ratio in $\log_e$ form
δ = ratio of rate of products formation to total rate of decomposition of activated acetone molecules
λ = wave length, Å. or cm.
ϕ_i = quantum yield of product or reaction i, g.moles/Einstein
( ) = denotes concentration, g.moles/cc.
tot = total for all wave lengths

LITERATURE CITED

1. Calvert, J. G., and J. N. Pitts, Jr., "Photochemistry," John Wiley, New York (1966).
2. Cassano, A. E., T. Matsuura, and J. M. Smith, *Ind. Eng. Chem. Fundamentals*, **7**, 655 (1968).
3. ———, and J. M. Smith, *AIChE J.*, **12**, 1124 (1966); **13**, 915 (1967).
4. Davis, W., Jr., *Chem. Rev.*, **40**, 201 (1947).
5. Baginsky, I. C., D. Eng. dissertation, Yale Univ., New Haven, Conn. (1951).
6. Gorin, E., *J. Chem. Phys*, **7**, 256 (1936).
7. Hanovia High-Pressure Quartz Mercury-Vapor Lamp Spectral Energy Distribution, Bull. EH-223.
8. Herr, D. S., and W. A. Noyes, Jr., *J. Amer. Chem. Soc.*, **62**, 2052 (1940).
9. Huff, J. E. and C. A. Walker, *AIChE J.*, **8**, 113 (1962).
10. Harris, P. R. and J. S. Dranoff, *ibid.*, **11**, 497 (1965).
11. Jacob, S. M., and J. S. Dranoff, *Chem. Eng. Prog. Symp. Ser.*, **62**, 47 (1966).
12. Luckey, G. W. and W. A. Noyes, Jr., *J. Chem. Phys.*, **19**, 227 (1951).
13. O'Neale, E. and S. Benson, *ibid.*, **36**, 2196 (1962).
14. Roebber, J. L., G. K. Rollefson, and G. C. Primentel, *J. Amer. Chem. Soc.*, **80**, 255 (1958).
15. Spence R. and W. Wild, *J. Chem Soc.*, 352 (1937); 590 (1941).
16. Steacie, E. W. R., "Atomic and Free Radical Reactions," Vol. I and II, Reinhold, New York (1954).

Manuscript received February 2, 1968; revision received April 26, 1968; paper accepted April 29, 1968.

APPENDIX

If a diffuse light pattern is assumed, radiation of uniform intensity, $I_{w,\lambda}$, will strike the reactor at any position across the diameter, as shown in Figure 1A. Further there will be equal probability of the light coming from any direction. It is sufficient, in this situation, to calculate the average light intensity over the cross-sectional area of the reactor by considering light from a single direction, as shown in the figure. This is true because the ratio of the average intensity for finite and zero absorptivities of acetone is the same whether calculated for light from a single direction or from all directions. In the calculations of $r_{d,c}$ from the data, only the ratio f is used, not the absolute intensity $\bar{I}$.

The attenuation of the light as it passes along any ray through the reactor, for example along AB, is determined by Lambert-Beer's law

$$\frac{dI_\lambda}{dx} = \mp \alpha_\lambda C_A I_\lambda \qquad (1A)$$

The total intensity at any point r, x is obtained by integrating Equation (1A) from the reactor wall to r, x in both directions along AB. The result is

$$I_\lambda(r,x) = I_{w,\lambda}\,[\exp\{-\alpha_\lambda C_A[(R^2-r^2)^{1/2}+x]\} + \exp\{-\alpha_\lambda C_A[(R^2-r^2)^{1/2}-x]\}] \qquad (2A)$$

The average intensity over the cross-sectional area is

$$\overline{I_\lambda} = \frac{I_{w,\lambda}}{\pi R^2}\int_{-R}^{R}\int_{-(R^2-x^2)^{1/2}}^{(R^2-x^2)^{1/2}} [\exp\{-\alpha_\lambda C_A[(R^2-r^2)^{1/2}+x]\} + \exp\{-\alpha_\lambda C_A[(R^2-r^2)^{1/2}-x]\}]\,dx\,dr \qquad (3A)$$

If a Taylor series expansion is used for the exponential terms, the integrated result is Equation (17).

Profiles of Laser-Created Cavities on Metal Surfaces

JOHN L. DEMING, JAMES H. WEBER, and LUH C. TAO

University of Nebraska, Lincoln, Nebraska

Metal surfaces of titanium, aluminum, copper, lead, and zinc were irradiated by a 25 joules pulsed laser with an energy flux ranging from 10^6 to 10^8 cal./(sq.cm.) (sec.). The resulted cavities were sectioned, polished and measured to compare with the isotherms computed from several heat conduction models. Reasonable agreement was found between the experimental cavity diameters at the interface and those calculated from the disk source model. Also, a graphical correlation between the cavity depth and its interface diameter is presented.

Laser beams are characterized by their high energy intensity, spatial and temporal coherence, and collimation. Among their many interesting applications are welding and drilling refractory materials and initiating exothermic chemical reactions. All involve the transport of an extremely high energy flux. Lindhom, Baker, Kirkpatrick (*8*) experimented with an electric arc source with a flux of 100 to 1,000 cal./(sq.cm.)(sec.) and found that the conventional theory of heat conduction is valid. The flux in this work is in the order of 10^9 to 10^8 cal./(sq. cm.)(sec.).

Bahun and Engquist (*2*) utilized the conventional heat transfer theory of point source to interpret the melting and vaporization of materials by the energy of a laser beam. Schmidt, Ham, and Hoshi (*10*) made micro hardness tests for the affected area of a metal irradiated by a focused laser beam. Anderson and Jackson (*1*) used the point source solution to illustrate the theory of welding. Ready (*9*) found by high speed photography that a plume of vaporized material started near the end of a laser pulse and that the measured vapor velocities of 2 to 5 $\times$ 10^4 cm./sec. were typical of materials from a boiling surface.

There have been no investigations on the profiles of laser-created cavities. This paper presents the results of

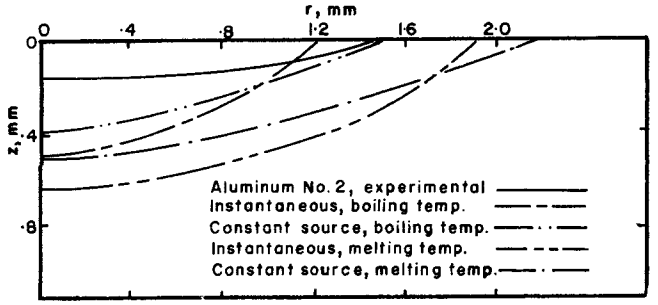

Fig. 1. Cavity profile and disk source isotherms.

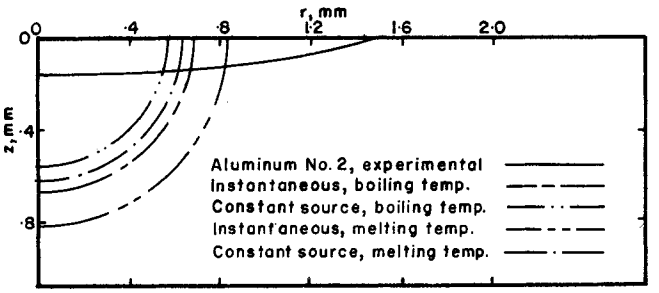

Fig. 2. Cavity profile and point source isotherms.

cavity profiles which are characterized by the diameters at the interface and the depths. The experimentally determined diameters at the interface were compared with those calculated by assuming various models based on heat conduction theory, and the depths were correlated empirically with the interface diameters.

MATHEMATICAL MODELS

The input of a very high energy flux is likely to cause a very high degree of superheat since time is essential for rearranging particles or aggregates during phase change. Thus, the irradiation of a laser pulse on a solid surface may assume the effect of heat conduction from a surface source without phase change during the short period of pulsing. Ready's observation (9) confirmed this fact. After the termination of the laser pulse, the temperature gradient near the surface in the solid phase would reverse in direction, causing a portion of the heat to flow from the plane of maximum temperature toward the surface. This provides the latent heat necessary to vaporize the material near the surface.

It is possible to calculate the location of isotherms by several energy source models before any phase change occurs, but probably only the melting point and boiling point isotherms may relate to the cavity profile. Since the latent heat required for a phase change is obtained from the sensible heat, the isotherm may become flat and move upward toward the interface while the temperature distribution at the interface may not be greatly affected by the phase change.

The energy transport in the solid phase is described by Equation (1) with the assumptions of a constant thermal diffusivity, absence of chemical reaction, no loss of energy by radiation and that the solid is opaque toward the laser light.

$$\partial T/\partial t = \kappa \nabla^2 T \qquad (1)$$

Since the total energy output of a laser beam can be controlled and the pulse time is 0.5 msec., six types of source models may be applicable. They are the point and the disk, indicating the spatial shape, and each one may be instantaneous, or constant, or a variable continuous source, indicating temporal shape of the energy source.

The solutions of instantaneous point and instantaneous disc sources in a semi-infinite medium are available (3). They are, respectively, rearranged in dimensionless forms:

$$T_1^* = [\exp(-z^{*2}/\theta^*)]/\pi^{1/2}\theta^{*3/2} \qquad (2)$$

$$T_1^* = [\exp(-z^{*2}/\theta^*)]\int_0^\infty \exp(-\theta^*\xi^2/4) J_0(\xi R^*) J_1(\xi) d\xi/\pi^{1/2}\theta^{*1/2} \qquad (3)$$

The continuous source solution can be obtained by integrating the instantaneous source solution after replacing Q in T_1^* by q (5). The solution in terms of dimensionless parameters is Equation (4):

$$T_2^*\theta^* = \int_0^{\theta^*} w(\theta^* - \bar{\theta}^*) T_1^*(\bar{\theta}^* - \theta^*) d\bar{\theta}^* \qquad (4)$$

The weighting factor $w(t) = q/\bar{q} = 1.0$ is for the constant source model.

Numerical solutions for Equations (2), (3) and the corresponding integrals of Equation (4) for constant sources have been calculated (4, 5). The pulse shape of the energy output of a laser beam (7) is known. However, the calculation results from the variable source model were very close to the corresponding ones from the constant source model. Consequently, the variable source model was not used in this paper.

EXPERIMENTAL EQUIPMENT AND PROCEDURE

A 15-QP Korad pulsed ruby laser was mounted on a horizontally leveled bench. It was aligned with a converging lens having a 5 cm. focal length and a sample holder. The sample holder was movable so that the laser beam could be focused to a predetermined diameter.

The ruby rod has a diameter of 9/16 in. which is also the diameter of the beam before focusing. The energy output of the laser at various power level settings were calibrated by a Korad calorimeter in conjunction with a Kiethley Model 150A microvoltmeter. Therefore, the controllable source strength and diameter of the laser beam were known parameters.

Commercially pure metals of lead, zinc, titanium, aluminum, and copper were chosen for the present study to cover a wide range of thermal diffusivities (at 20°C.) which are respectively 0.24, 0.40, 0.657, 0.90, and 1.14 sq.cm./sec. (6). The thermal conductivity measured at low energy flux may be different from that at a very high flux because of the very short time of pulsing, which would not allow the material to reach the normal arrangement at low energy flux. Because of this uncertainty, computations used only the thermal diffusivities at room temperature without any adjustment of their temperature dependence.

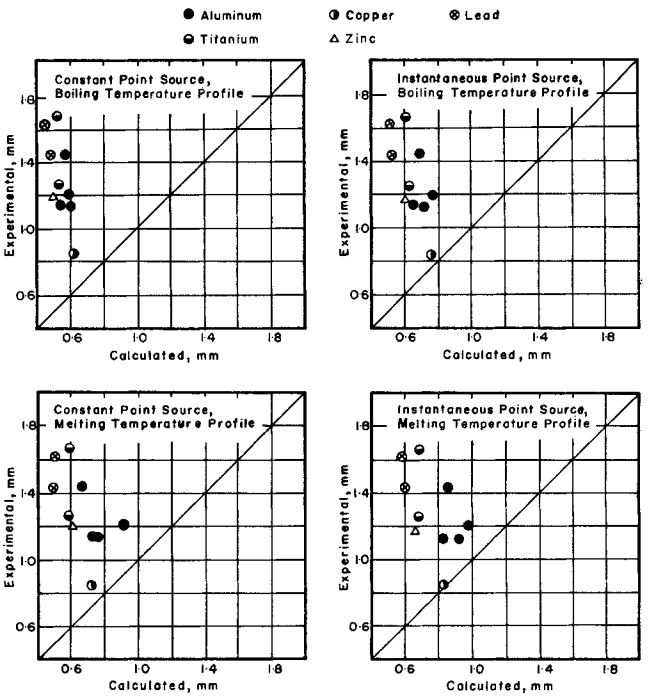

Fig. 3. A comparison of cavity radii. Experimental vs. estimated from point source models.

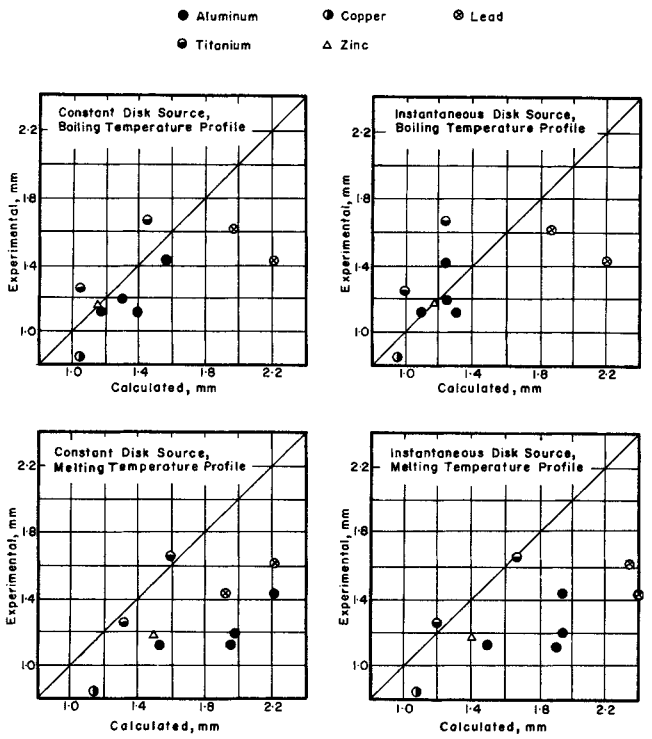

Fig. 4. A comparison of cavity radii. Experimental vs. estimated from disk source models.

Surfaces of metal samples with thickness of 5 to 8 mm. were smoothed successively by 240, 320, 400, and 600 grit sand papers. After cleaning with a dry cloth, the samples were allowed to oxidize slightly in the room air and then stored in a desiccator. The irradiated samples were photographed by using a metallograph. The 25× magnified photographs were used in measuring the cavity diameters at the interface. Samples were then milled parallel to the cavity axes. About 0.005 in. were allowed in milling so that further polishing and etching would result in exposing the cavity profiles along their axes. The specimens were then polished sequentially with 240, 320, 400, and 600 grit papers and a felt using 0.05μ aluminum oxide. Finally, chemical etching was used to expose the microstructure. The exact profiles were then determined from the 100× photographs.

RESULTS

Tabulation of experiments, results, and photographs are available (*4*). Only significant findings related to the cavity profile will be presented here.

Figures 1 and 2 show the comparison between a typical cavity profile and the computed boiling temperature and melting temperature isotherms. The experimental profile was relatively flat as predicted by the previous discussion. Deviations of the cavity profile from the isotherms are large at the cavity axis. The melting point isotherm of the disk source predicts a larger cavity diameter at the surface than the experimental one. This indicates that the vaporization of metal produced the cavity and the molten metal at the cavity periphery probably stayed *in situ*.

The experimental cavity diameters and the corresponding ones calculated from the point source models are plotted in Figure 3. This graph indicates that the point source model is unsatisfactory. However, Figure 4 shows that using the constant disk source model in conjunction with the boiling temperature profile gives diameters in fair agreement with the experimental data. This implies that the cavity was probably formed as a result of superheating and then followed by vaporization of the metal.

DISCUSSIONS

For the purpose of calculating the location of the isotherm profiles, an assumption was made that all the energy of the focused laser beam was absorbed by the metal. Since an experimental determination of absorptivity of these metals to the 6,943 Å. light of the laser beam could not be made in our laboratory, this assumption could not be checked and might cause some error in the computed diameters. The absorptivity would be different for different materials as shown in Figure 4 which does indicate some degree of segregation between the results obtained from the various metals. However, some of these variations might be caused by the irregularity of the cavity shape. Therefore, the absorptivity assumption may not affect the computed results seriously.

The validity of the assumption, made in all instances, that the sample may be regarded as a semi-infinite medium was established by calculating the temperature gradients which would exist under severe conditions. For example, the cavity depth in the lead sample was 0.37 mm., but at a depth of somewhat less than 0.70 mm. ambient temperature existed.

Since both the surface diameter and the depth of cavity are functions of the same groups of physical properties of metals and operating conditions, a correlation may exist if they are arranged in the forms of dimensionless groups. Figure 5 shows this empirical correlation between the dimensionless radius and depth. Therefore, from the disk source model and this correlation, the profile of a laser-created cavity can be characterized and sketched.

CONCLUSIONS

The diameter of a laser-created cavity can be predicted by using a constant disk source model for heat conduction in solids. A correlation was also found to predict the cavity depth. Also, it provides a method to predict the approximate size of a cavity caused by laser irradiation.

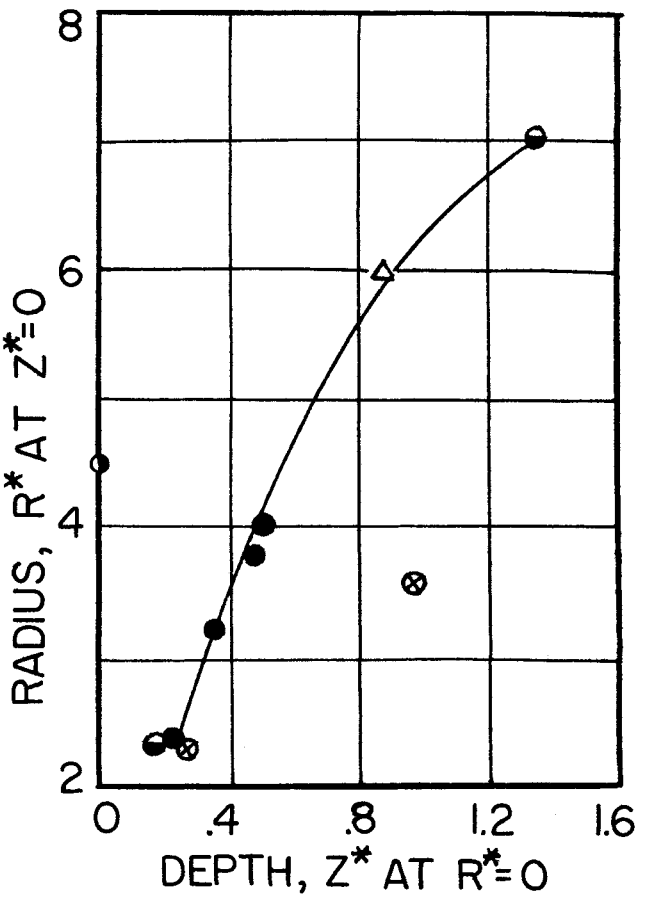

Fig. 5. Dimensionless radii vs. depths of cavities. ● aluminum, ◑ copper, ⊗ lead, ◒ titanium, △ zinc.

ACKNOWLEDGMENT

This work was supported by NSF grant No. GK-455 and a National Aeronautics and Space Administration fellowship to John L. Deming.

NOTATION

C_p = heat capacity of solid
q = source energy per unit time
$\overline{q}$ = average source energy per unit time
Q = energy of the source
r = radial distance
R = radius of laser beam at the solid surface
R^* = dimensionless radius, r/R
t = time
T = temperature
T_1^* = dimensionless time, $T\rho C_p \pi R^3/2Q$
T_2^* = dimensionless time, defined by Equation (4)
w = weighting factor
z = axial distance
Z^* = dimensionless depth, z/R

Greek Letters

θ^* = dimensionless time, $4\kappa t/R^2$
$\overline{\theta^*}$ = dummy variable in Equation (4)
κ = thermal diffusivity
ξ = dimensionless variable, λR (3, 4)
ρ = density of solid

LITERATURE CITED

1. Anderson, J. E., and J. E. Jackson, *Welding J.*, 44, 1018 (1965).
2. Bahun, C. J., and R. D. Engquist, *Metals Eng., Quart.*, 27 (Feb., 1964).
3. Carslaw, H. S., and J. C. Jaeger, "Conduction of Heat in Solids," 2nd Ed. p. 258 to 60, Oxford Press, New York (1959).
4. Deming, J. L., MS thesis, Univ. Nebraska, Lincoln (1967).
5. ———, and L. C. Tao, and J. H. Weber, *AIChE J.*, 13, 1214 (1967).
6. Hampel, C. A., "Rare Metals Handbook," p. 635, Rheinhold Publ. Corp., New York (1954).
7. "Instruction Manual For Model K-150QP Laser," p. 1, Korad Corporation, Santa Monica, Calif. (1965).
8. Lindholm, U. S., E. J. Baker, and R. C. Kirkpatrick, *J. Heat Transfer*, 87, 49 (1965).
9. Ready, J. F., *Appl. Phys. Letters*, 3, 11 (1963).
10. Schmidt, A. O., I. Ham, and T. Hoshi, *Welding J. Res. Suppl.*, 44, 481 (1965).

Manuscript received October 24, 1967; revision received March 15, 1968; paper accepted April 26, 1968.

Laminar, Nonisothermal Flow of Fluids in Tubes of Circular Cross Section

E. B. CHRISTIANSEN and GORDON E. JENSEN

University of Utah, Salt Lake City, Utah

Numerical solutions of the equations of motion and energy are presented in the form of pressure-loss, flow-rate relationships for the laminar, nonisothermal flow of Newtonian and non-Newtonian fluids being heated and cooled in tubes at constant wall temperature. The flow properties are represented by a temperature-dependent form of the power law equation. The numerical results are shown to be in good agreement with experimental data for a wide range of fluid properties and flow conditions.

The heating and cooling of Newtonian and, especially, non-Newtonian fluids in laminar flow in tubes of circular cross section are becoming increasingly important in the chemical process industries. With few exceptions, presently available methods for the prediction of the pressure-gradient flow-rate relations for laminar, nonisothermal flow of Newtonian and non-Newtonian fluids in tubes of circular cross section employ the empirical Sieder-Tate type of corrections to introduce the effect of temperature on the flow of the fluid (*9, 14, 15*). While such methods are often satisfactory, extrapolation beyond the range of the data on which they are based may introduce serious error. Recently, a numerical solution of restricted equations of motion and energy which provides pressure-gradient flow-rate data for the laminar flow of non-Newtonian fluids being heated in tubes was reported (*5, 6*), in which a temperature-dependent form of the Ostwald-de Waele power law equation,

$$\tau = m[\dot{S} \exp(\Delta H^{\ddagger}/RT)]^n \qquad (1)$$

was used to represent the flow of the fluid. This equation is reported (*1, 12*) to represent quite accurately the flow of nonassociating Newtonian fluids ($n = 1$). Although, for pseudoplastic fluids ($n < 1.0$), Equation (1) predicts unrealistically high apparent viscosities at very low shear rates and unrealistically low apparent viscosities at very high shear rates, it correctly represents the flow of some non-Newtonian fluids over extended ranges of temperatures and shear rates (*2, 10*); and it represents the steady state flow of most non-Newtonian fluids over relatively narrow but significant and useful shear rate and tempera-

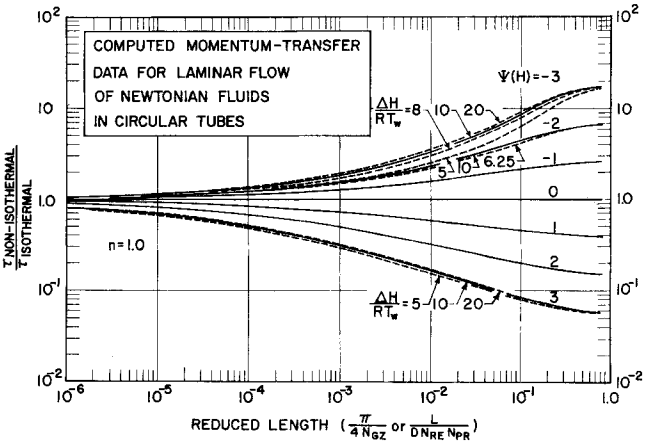

Fig. 1. Computed functions for Newtonian flow, $n = 1$. Positive values of $\Psi(H)$ represent energy transfer to the fluid, and negative values represent energy transfer from the fluid. The solid lines are for $\Delta H^{\ddagger}/RT_R = 10$. Dashed lines are included for $\Delta H^{\ddagger}/RT_R = 5$ to 20, when the function for these values differed by more than 2% from the function for $\Delta H^{\ddagger}/RT_R = 10$.

Gordon E. Jensen is with the United Technology Center, Sunnyvale, California.